

Radiative corrections and parity-violating electron-nucleon scattering

S. Barkanova¹, A. Aleksejevs¹, and P.G. Blunden^{1,2}

¹*Department of Physics and Astronomy, University of Manitoba, Winnipeg, MB, Canada
R3T 2N2*

²*Jefferson Laboratory, 12000 Jefferson Avenue, Newport News, VA 23606*

Abstract

Radiative corrections to the parity-violating asymmetry measured in elastic electron-proton scattering are analyzed in the framework of the Standard Model. We include the complete set of one-loop contributions to one quark current amplitudes. The contribution of soft photon emission to the asymmetry is also calculated, giving final results free of infrared divergences. The one quark radiative corrections, when combined with previous work on many quark effects and recent SAMPLE experimental data, are used to place some new constraints on electroweak form factors of the nucleon.

12.15.Ji,12.15.Lk,13.40.Ks,25.30.Bf

I. INTRODUCTION

One of the areas of active theoretical and experimental interest is in understanding the strange quark contribution to nucleon electroweak form factors. The s quarks are a key to the overall sea properties, and their distribution is of particular interest for developing our understanding of low energy nucleon structure. At present, theoretical estimates of strangeness electric and magnetic form factors span a wide spectrum in both magnitude and sign [1].

The electromagnetic current is a pure $SU(3)_f$ octet. By exploiting flavor symmetries one can separate two flavor structures: the isovector, $(u - d)$, and the hypercharge, $(u + d - 2s)$. There is no singlet component $(u + d + s)$, so the electromagnetic current can not provide sufficient information to separate u , d , and s contributions.

The Z^0 offers a new flavor coupling to the nucleon proportional to weak isospin, which samples $(u - d - s)$ in the light quark sector. Knowing matrix elements of $(u - d)$, the Z^0 can be used as a probe to find strange quark matrix elements in the nucleon [2]. One can measure such direct characteristics of strangeness in the nucleon as the strange magnetic moment $\mu_s = \frac{1}{2}s^\dagger \mathbf{r} \times \boldsymbol{\alpha} s$, the strangeness charge radius $r_s^2 = s^\dagger r^2 s$, and the strangeness analog of the axial charge $\bar{s} \boldsymbol{\gamma} \gamma_5 s$, which can serve as an independent confirmation of the quark spin fraction measurements.

Electroweak properties of the nucleon can be studied by parity-violating electron scattering at low to medium energies [3]. There the asymmetry factor coming from the difference between cross sections of left- and right-handed electrons can be measured. However, extracting information of interest from the experimental data requires evaluating radiative corrections to electroweak scattering at the few percent level.

Electroweak radiative corrections to intermediate energy, parity non-conserving semi-leptonic neutral current interactions have been addressed previously [4–8]. In these works, radiative corrections are constructed from the underlying fundamental weak interaction between electron and quarks. Broadly, such corrections are denoted as being either one-quark or many-quark effects. The one-quark corrections involve the interaction of the electron with a single quark. The many-quark contributions involve two or more quarks, and include effects due to an intrinsic weak interaction in the nucleon (e.g. the anapole moment). In this work, we restrict our considerations to the one-quark contributions.

The use of computer packages *FeynArts*, *FormCalc*, and *LoopTools* [9] is of great assistance in facilitating our calculations, allowing us to include the full set of one-loop contributions (there are several hundred Feynman diagrams, which are laborious to calculate by hand), and to retain the momentum-dependence of the amplitudes, for example. Our treatment of hadronic model dependencies (e.g. kinematics) is slightly different than previous work. In addition, we have treated infrared (IR) divergences in the one-loop amplitudes by including bremsstrahlung contributions for soft photon emission. While such a prescription is not completely satisfactory, and would be better handled by also accounting for hard photons and the particular detector setup of a given experiment, it nevertheless sets the scale for uncertainties of this origin.

The article is described as follows. In Sec. II we give the formalism for parity-violating electron scattering, including definitions of the relevant currents, couplings, form factors, and kinematics. Section III outlines the one-loop calculations, including the prescription for

including soft photon emission. Results for the radiative corrections are given in Sec. IV. Finally, our results are combined with other calculations of many-quark effects to discuss the implications for the SAMPLE experiment.

II. FORMALISM

A. Parity violating electron scattering

At tree level, the electron-nucleon scattering amplitude consists of two terms, \mathcal{M}^γ (Fig. 1a) and \mathcal{M}^Z (Fig. 1b). The first term is parity-conserving γ -exchange, and the sec-

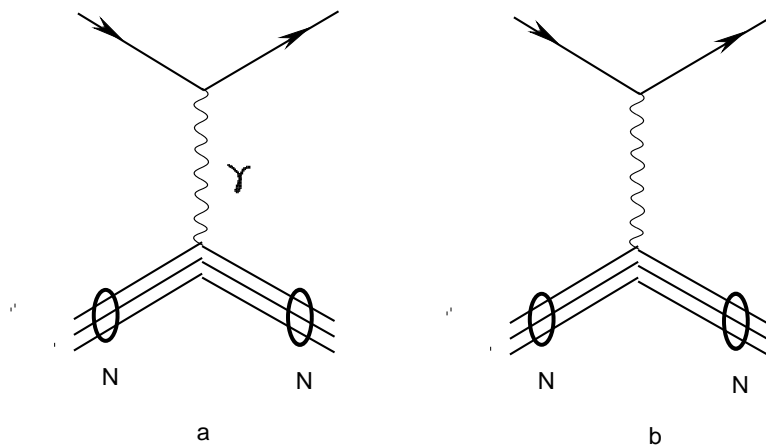


FIG. 1. Tree level electron-nucleon scattering.

ond has a parity-violating contribution from Z^0 -exchange. The differential cross section is proportional to

$$d\sigma \sim |\mathcal{M}^\gamma + \mathcal{M}^Z|^2 = |\mathcal{M}^\gamma|^2 + 2\text{Re}\{(\mathcal{M}^\gamma)^* \mathcal{M}^Z\} + |\mathcal{M}^Z|^2. \quad (2.1)$$

The purely weak term $|\mathcal{M}^Z|^2$ is very small compared to the other terms and can safely be neglected. The electromagnetic-weak interference term $2\text{Re}\{(\mathcal{M}^\gamma)^* \mathcal{M}^Z\}$ contains the physics of interest. This term can be extracted from the parity-violating asymmetry, formed as the ratio of helicity-dependent to helicity-independent cross sections:

$$\mathcal{A} = \frac{d\sigma_R - d\sigma_L}{d\sigma_R + d\sigma_L}. \quad (2.2)$$

Here, σ_R and σ_L are cross sections for right- and left-handed electrons, respectively. This ratio, measured in a number of experiments, is of the order 10^{-6} at low energies.

For elastic electron-nucleon scattering, the asymmetry ratio is given by [7,10]

$$\begin{aligned} \mathcal{A} &= \left[\frac{-G_F Q^2}{4\sqrt{2}\pi\alpha} \right] \frac{\varepsilon G_E^\gamma G_E^Z + \tau G_M^\gamma G_M^Z - (1 - 4\sin^2\theta_W)\varepsilon' G_M^\gamma G_A^Z}{\varepsilon(G_E^\gamma)^2 + \tau(G_M^\gamma)^2} \\ &\equiv -\frac{G_F Q^2}{4\sqrt{2}\pi\alpha} \times \frac{N}{D}, \end{aligned} \quad (2.3)$$

where $Q^2 > 0$ is the four-momentum transfer. G_E^γ and G_M^γ are the electric and magnetic vector form factors of the nucleon associated with γ -exchange, G_E^Z and G_M^Z are the similar parameters for Z^0 -exchange, and G_A^Z is the axial vector form factor. Kinematic parameters τ , ε and ε' are defined as

$$\begin{aligned} \tau &= \frac{Q^2}{4M_N^2}, \\ \varepsilon &= \frac{1}{1 + 2(1 + \tau)\tan^2\frac{\theta}{2}}, \\ \varepsilon' &= \sqrt{\tau(1 + \tau)(1 - \varepsilon^2)}. \end{aligned} \quad (2.4)$$

The electromagnetic vector form factors of the proton $G_E^{\gamma,p}$ and $G_M^{\gamma,p}$ are well measured, and some constraints can be put on $G_E^{\gamma,n}$ and $G_M^{\gamma,n}$ for the neutron [11]. The expressions for the weak form factors of the nucleon, G_E^Z and G_M^Z , and the axial vector coupling G_A^Z , are given below. The factor $(1 - 4\sin^2\theta_W) \simeq 0.1$ suppresses the term containing G_A^Z , and makes the contribution of higher order processes more apparent.

The neutral weak vector form factors for the proton and neutron can be expressed in terms of the electromagnetic form factors of the proton and neutron, plus a contribution from strange quarks [12]. We choose to write this in the form

$$\begin{aligned} G_{E,M}^Z &= (1 - 2\sin^2\theta_W) \left[1 + R_V^{T=1} \right] G_{E,M}^{T=1\tau_3} \\ &\quad - 2\sin^2\theta_W \left[1 + R_V^{T=0} \right] G_{E,M}^{T=0} - \left[1 + R_V^{(0)} \right] G_{E,M}^s. \end{aligned} \quad (2.5)$$

Here $R_V^{T=0}$, $R_V^{T=1}$, and $R_V^{(0)}$ are the isoscalar, isovector, and isosinglet weak radiative corrections describing the contribution from weak vector couplings beyond tree level, respectively. Strong isospin τ_3 is equal to $+1(-1)$ for the proton (neutron). The isoscalar and isovector electromagnetic form factors are taken to be the linear combinations

$$\begin{aligned} G_{E,M}^{T=0} &= G_{E,M}^p + G_{E,M}^n, \\ G_{E,M}^{T=1} &= G_{E,M}^p - G_{E,M}^n, \end{aligned} \quad (2.6)$$

so that at $Q^2 = 0$, $G_E^{T=0}(0) = G_E^{T=1}(0) = 1$, and $G_M^{T=0}(0) = 0.8797$, $G_M^{T=1}(0) = 4.709$. The strange quark form factors are undetermined, but take on the values $G_E^s(0) = 0$ and $G_M^s(0) = \mu_s$, where μ_s is the contribution of strange quarks to the magnetic moment of the nucleon.

The axial vector coupling is conveniently written in terms of octet matrix elements [7] as

$$G_A^Z = - \left[1 + R_A^{T=1} \right] G_A^{T=1} \tau_3 + \sqrt{3} R_A^{T=0} G_A^{(8)} + \left[1 + R_A^{(0)} \right] G_A^s. \quad (2.7)$$

The isovector axial form factor $G_A^{T=1}$ is determined from neutron beta decay as $G_A^{T=1}(0) = g_A$, with $g_A = 1.2670 \pm 0.0035$. The second term involving the $SU(3)$ isoscalar octet form factor $G_A^{(8)}$ is not present at tree level. From a least squares fit to hyperon beta decay, we have determined $G_A^{(8)} = 0.169 \pm 0.009$, which is consistent with results of polarized deep inelastic lepton scattering [13]. In our calculations (see section IV) we find $|R_A^{T=0}| < |R_A^{T=1}|$, so we expect overall that the second term in Eq. (2.7) is suppressed relative to the first term. The axial strange form factor G_A^s is extracted from polarized deep inelastic lepton scattering as $G_A^s(Q^2 = 0) = -0.086 \pm 0.024$ [13]. Due to the unknown Q^2 dependence we take $G_A^s(Q^2 = 0.1) = -0.086 \pm 0.086$ in our analysis.

Additional information on the axial vector form factor can be provided by parity-violating quasielastic scattering from deuterium. In the simplest impulse approximation, the asymmetry ratio for the deuteron can be written as the incoherent sum of neutron and proton contributions

$$\mathcal{A}_d = \left[\frac{-G_F Q^2}{4\sqrt{2}\pi\alpha} \right] \frac{N_n + N_p}{D_n + D_p}, \quad (2.8)$$

where $N_p(N_n)$ is the numerator and $D_p(D_n)$ is the denominator in Eq. (2.3) for the proton (neutron).

B. Radiative effects

As was indicated in the previous section, extracting form factors $G_{E,M}^Z$ and G_A^Z is based not only on experimental data, but also on theoretical calculations of radiative corrections for parity-violating scattering. We calculate the radiative corrections to tree level for the electroweak interaction in the scattering processes $e + p \rightarrow e + p$ and $e + n \rightarrow e + n$ by modeling the nucleon as a collection of quasi-free quarks carrying some fraction x of the nucleon four-momentum.

If we assume that during the scattering process the electron interacts with only one quark, we can split the problem of electron-nucleon scattering into calculations of Feynman graphs for processes like $e(p_1) + q(p_2) \rightarrow e(p_3) + q(p_4)$, with q representing (u, d, s) quarks. Starting from the fundamental coupling of an elementary fermion to the photon or to the Z^0 , one can arrive at the general form of electromagnetic and weak invariant amplitudes [7]:

$$\mathcal{M}^\gamma = -\frac{4\pi\alpha}{q^2} Q_f l^\mu J_\mu^\gamma, \quad (2.9a)$$

$$\mathcal{M}^Z = -\frac{4\pi\alpha}{M_Z^2 - q^2} \frac{1}{(4 \sin \theta_W \cos \theta_W)^2} \left(g_V^f l^\mu + g_A^f l^{\mu 5} \right) \left(J_\mu^Z + J_{\mu 5}^Z \right), \quad (2.9b)$$

where l^μ ($l^{\mu 5}$) and J^μ ($J^{\mu 5}$) are leptonic and hadronic vector (axial vector) currents, respectively, and Q_f is the electromagnetic charge number of the fermion.

The weak coupling has been expressed in terms of the set (α, M_W, M_Z) rather than G_F , noting that $\sin^2 \theta_W = 1 - M_W^2/M_Z^2$ in our renormalization scheme. The vector and axial-vector ‘‘charges’’ of the fermion, g_V^f and g_A^f , are defined as

$$g_V^f = 2T_3^f - 4Q_f \sin^2 \theta_W, \quad (2.10a)$$

$$g_A^f = -2T_3^f, \quad (2.10b)$$

with $T_3^f = +\frac{1}{2}(-\frac{1}{2})$ for the upper (lower) member of the fermion doublet.

Explicitly, we have for the electron and the (u, d, s) quarks:

$$\begin{aligned} g_V^e &= -1 + 4 \sin^2 \theta_W, & g_A^e &= +1, \\ g_V^u &= +1 - \frac{8}{3} \sin^2 \theta_W, & g_A^u &= -1, \\ g_V^{d,s} &= -1 + \frac{4}{3} \sin^2 \theta_W, & g_A^{d,s} &= +1. \end{aligned} \quad (2.11)$$

For the case of electron scattering, leptonic vector and axial-vector currents are Dirac currents with electron spinor u_e :

$$l^\mu = \bar{u}_e \gamma^\mu u_e, \quad (2.12a)$$

$$l^{\mu 5} = \bar{u}_e \gamma^\mu \gamma^5 u_e. \quad (2.12b)$$

Hadronic currents J_μ are hadronic matrix elements of the electro-magnetic, vector, and axial-vector quark current operators:

$$J_\mu = \langle N | \hat{J}_\mu | N \rangle, \quad (2.13)$$

($J_\mu = J_\mu^\gamma, J_\mu^Z$ or $J_{\mu 5}^Z$; $|N\rangle = |p\rangle$ or $|n\rangle$),

$$\begin{aligned} \hat{J}_\mu^\gamma &= \sum_q Q_q \bar{u}_q \gamma_\mu u_q, \\ \hat{J}_\mu^Z &= \sum_q g_V^q \bar{u}_q \gamma_\mu u_q, \\ \hat{J}_{\mu 5}^Z &= \sum_q g_A^q \bar{u}_q \gamma_\mu \gamma_5 u_q. \end{aligned} \quad (2.14)$$

Nominally, summation must be done over all quark flavors, but it is sufficient at the momentum scale of interest to include only light quarks, $u, d,$ and s . In order to be parity-violating, Z^0 exchange must involve either $V(e) \times A(q)$ or $A(e) \times V(q)$. Thus, it is convenient to express the amplitude for the parity-violating (PV) part of the electron-quark (eq) scattering in the general form

$$\begin{aligned} \mathcal{M}_{PV}^{eq} &= A^{eq} \bar{u}_e(p_3) \gamma^\mu u_e(p_1) \cdot \bar{u}_q(p_4) \gamma_\mu \gamma_5 u_q(p_2) \\ &\quad + B^{eq} \bar{u}_e(p_3) \gamma^\mu \gamma_5 u_e(p_1) \cdot \bar{u}_q(p_4) \gamma_\mu u_q(p_2), \\ &\equiv A^{eq} J_{VA}^{eq} + B^{eq} J_{AV}^{eq}. \end{aligned} \quad (2.15)$$

Here, A^{eq} and B^{eq} are functions of the Standard Model parameters, n -point tensor coefficients, and kinematics. From this point we define one-loop radiative correction to tree level electron-quark scattering as follows:

$$R_A^q \equiv \frac{A_{\text{rad}}^{eq}}{A_{\text{tree}}^{eq}}, \quad R_V^q \equiv \frac{B_{\text{rad}}^{eq}}{B_{\text{tree}}^{eq}}, \quad (2.16)$$

where A_{tree}^{eq} and B_{tree}^{eq} come from the tree level, and A_{rad}^{eq} and B_{rad}^{eq} come from the one-loop radiative corrections. The relationship between the hadronic radiative corrections of Eqs. (2.5-2.7) and the electron-quark radiative corrections of Eq. (2.16) follows from the linear combinations:

$$\begin{aligned} R_V^{T=0} &= (g_V^u R_V^u + g_V^d R_V^d)/(g_V^u + g_V^d), \\ R_V^{T=1} &= (g_V^u R_V^u - g_V^d R_V^d)/(g_V^u - g_V^d), \\ R_V^{(0)} &= (g_V^u R_V^u + g_V^d R_V^d + g_V^s R_V^s)/(g_V^u + g_V^d + g_V^s), \\ R_A^{T=0} &= -R_A^u + R_A^d, \\ R_A^{T=1} &= (R_A^u + R_A^d)/2, \\ R_A^{(0)} &= -R_A^u + R_A^d + R_A^s. \end{aligned} \quad (2.17)$$

For the axial corrections we have used the explicit values of g_A^q , which are $+1$ or -1 , and the $R_A^{T=0}$ correction is calibrated to 1, since the tree level term $g_A^u + g_A^d = 0$.

Each particle carries 4-momentum $p_i^2 = m_i^2$ with the following structure in the center-of-mass (CM) frame:

$$\begin{aligned} p_1 &= (E_1, 0, 0, p), \\ p_2 &= (E_2, 0, 0, -p), \\ p_3 &= (E_3, p \sin \theta, 0, p \cos \theta), \\ p_4 &= (E_4, -p \sin \theta, 0, -p \cos \theta). \end{aligned} \quad (2.18)$$

Here $E_1 = E_3$ and $E_2 = E_4$ (for elastic scattering) and p denote the energy and momentum of the scattered particles. The Mandelstam variables are defined as follows:

$$\begin{aligned} s &= (p_1 + p_2)^2 = (E_1 + E_2)^2 = E_{\text{CM}}^2, \\ t &= (p_1 - p_3)^2 = -2p^2(1 - \cos \theta), \\ u &= (p_1 - p_4)^2 = (E_1 - E_2)^2 - 2p^2(1 + \cos \theta), \end{aligned} \quad (2.19)$$

with $E_{1,2}^2 = p^2 + m_{1,2}^2$. For elastic scattering we have $s + t + u = 2m_1 + 2m_2$. Input kinematic parameters, in our case, are the energy of the electron in the laboratory reference frame, E_{lab} , and the scattering angle θ . Hence E_{CM} and p can be expressed in terms of E_{lab} and θ :

$$p^2 = \frac{(E_{\text{CM}}^2 + m_2^2 - m_1^2)^2}{2E_{\text{CM}}^2} - m_2^2. \quad (2.20)$$

For quarks bound in the nucleon, we can assume that the energy of the quark can be defined as a fraction of the mass of the nucleon $E_{2,\text{lab}}^2 = x^2 m_N^2$, with $x \approx 1/3$. Taking into account $E_{2,\text{lab}}^2 = p_{2,\text{lab}}^2 + m_2^2$, we can determine center-of-mass energy as follows:

$$\begin{aligned} E_{\text{CM}}^2 &= (p_{1,\text{lab}} + p_{2,\text{lab}})^2 \\ &= m_1^2 + m_2^2 + 2E_{1,\text{lab}} x m_N \left(1 - \frac{(E_{1,\text{lab}}^2 - m_1^2)^{1/2} ((x m_N)^2 - m_2^2)^{1/2} \cos \theta_i}{E_{1,\text{lab}} x m_N} \right). \end{aligned} \quad (2.21)$$

In the latter equation, θ_i denotes the unknown angle between the spatial momentum of the electron and quark just before scattering took place. Final expressions for radiative corrections have been integrated over this angle to account for all possible values of θ_i .

III. DETAILS OF THE CALCULATION

A. One-loop corrections

Doing one-loop calculations in the Standard Model by hand is a laborious task due to the sheer number of particles and the complexity of the underlying theory. To facilitate this task, and to reduce the possibility of errors, for some time software packages have been developed to automate different tasks in these calculations [14]. In this paper, we have chosen to use the packages *FeynArts*, *FormCalc*, and *LoopTools* [9]. These packages are designed to work hand in hand on various aspects of the calculation, as described below.

In total, 438 one-loop diagrams were calculated, including counterterms and contributions from scalar bosons (H, χ, ϕ) and ghost fields (u_Z, u_-, u_+). For analysis and comparison with earlier work (see Ref. [4], for example), it is useful to split diagrams into three classes (Fig. 2). Class 1 are self-energy loops, Class 2 are triangles, and Class 3 are boxes. Class 1 have a dominant contribution from Z exchange and γZ mixing. Class 2 include triangles with $ff'Z$ and $ff'\gamma$ vertices. Class 3 are the ZZ , WW and γZ box and crossed box diagrams. Contributions from scalar bosons and ghost fields to the boxes were found to be negligibly small.

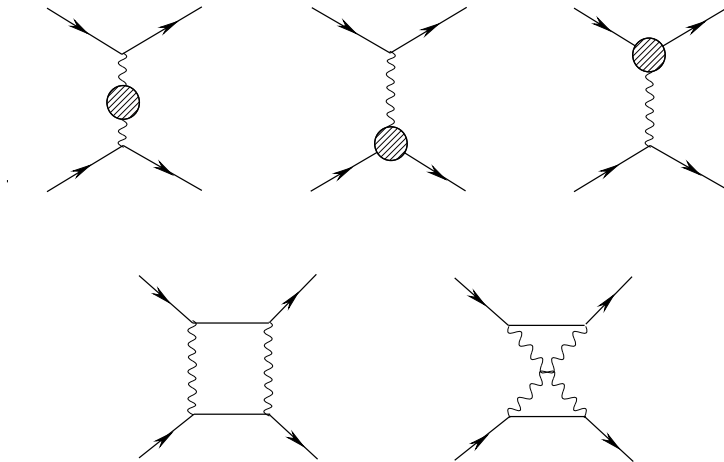


FIG. 2. Classes of one-loop contributions to electron-quark scattering include self-energy, vertex, and box diagrams.

Because of the huge size of the analytical expressions for amplitudes, we leave them out of this article. Certain steps involved in the evaluation of one-loop PNC amplitude have to be explained more carefully. To evaluate four dimensional one-loop tensor integrals, we have used the Constrained Differential Renormalization (CDR) scheme [15] implemented in the package *FormCalc*. In the CDR scheme, Feynman diagrams are considered completely in four dimensions. Thereafter, the reduction of singular basic functions (products of propagators and their derivatives) has been renormalized into the sum of “regular” ones by implementing a set of rules in such a way that Ward identities are satisfied. It was proven in Ref. [9] that CDR is equivalent at the one-loop level to regularization by dimensional reduction [16], after taking the Fourier transform of the basic renormalized functions into momentum space. This last approach corresponds to a modified dimensional regularization, where one-loop integrals are considered in D dimensions, but all the tensors and spinors are kept 4-dimensional [16]. To preserve gauge invariance in dimensional reduction, one should use $\hat{g}_{\mu\nu}$ ($\hat{g}_\mu^\mu = D$) with $g_{\mu\nu}\hat{g}^{\nu\rho} = \hat{g}_\mu^\rho$ for the tensor decomposition.

In dimensional regularization, the general structure of one-loop tensor integral can be written in the form [17]

$$J_{i_1\dots i_p}^N = \frac{(2\pi\mu)^{4-D}}{i\pi^2} \int d^D q \frac{q_{i_1} q_{i_2} \dots q_{i_p}}{(q^2 - m_1^2) ((q + p_1)^2 - m_2^2) \dots ((q + p_{N-1})^2 - m_N^2)}. \quad (3.1)$$

Here, (μ) means the regularization scale parameter of dimensional reduction, which is related to the CDR renormalization scale by $\log(\bar{M}^2) = \log(\mu^2) + 2$. For the tensor decomposition of Eq. (3.1) into linear combinations of tensor coefficient functions, we have used the method of Passarino-Veltman [18].

The Passarino-Veltman approach deals with two, three, and four point tensor integrals with two, three, and four propagators, respectively. The rank of the tensors is equal to the number of integrable momenta ($q_{i_1} q_{i_2} \dots q_{i_p}$) in the numerator of Eq. (3.1). Two, three and four point tensor coefficient functions, coming from tensor decomposition, were calculated numerically by using the package *LoopTools*, and algebraic calculations were completed with the help of packages *FeynArts*, *FormCalc* and *FORM*. To summarize this section, we provide an outline of how calculations were implemented in these packages.

Generation of the diagrams (package *FeynArts*)

- Topologies are defined
- Fields are inserted
- Amplitudes and their counterterms in integral form were defined, along with CKM matrix

Evaluation of amplitudes (package *FormCalc* along with *FORM*)

- Indices contracted and traces are taken
- Amplitudes in general form (i.e. combination of many-point tensor coefficients along with spinor chains) were presented

- Radiative corrections were calculated (On Shell Renormalization)
- Infrared divergences are treated by adding soft-photon emission

Numerical evaluation

- Standard Model parameters and kinematics are defined
- Many-point tensor coefficients are numerically evaluated (package *LoopTools*)

B. Renormalization constants

Generally, tensor coefficient functions are ultraviolet divergent (inversely proportional to the parameter $\varepsilon = 4 - D$). In order to cancel divergences and transform bare parameters into physical observables one has to introduce a renormalization scheme. The renormalized parameters are related to the bare parameters (denoted by a subscript 0) as follows:

$$\begin{aligned}
M_{Z,0}^2 &= M_Z^2 + \delta M_Z^2, \\
M_{W,0}^2 &= M_W^2 + \delta M_W^2, \\
M_{H,0}^2 &= M_H^2 + \delta M_H^2, \\
m_{f_i,0} &= m_{f_i} + \delta m_{f_i}, \\
e_0 &= (1 + \delta e) e, \\
\begin{pmatrix} Z_0 \\ A_0 \end{pmatrix} &= \begin{pmatrix} 1 + \frac{1}{2}\delta Z^{ZZ} & \frac{1}{2}\delta Z^{ZA} \\ \frac{1}{2}\delta Z^{AZ} & 1 + \frac{1}{2}\delta Z^{AA} \end{pmatrix} \begin{pmatrix} Z \\ A \end{pmatrix}, \\
W_0^\pm &= \left(1 + \frac{1}{2}\delta Z^{WW}\right) W^\pm, \\
H_0 &= \left(1 + \frac{1}{2}\delta Z^H\right) H, \\
f_{i,0}^L &= \left(\delta_{ij} + \frac{1}{2}\delta Z_{ij}^{f,L}\right) f_j^L, \\
f_{i,0}^R &= \left(\delta_{ij} + \frac{1}{2}\delta Z_{ij}^{f,R}\right) f_j^R.
\end{aligned} \tag{3.2}$$

Counterterms were chosen in the On Shell Renormalization (OSR) scheme in the 't Hooft-Feynman gauge, where the gauge parameter $\xi = 1$. The renormalization constants are [19]:

Wave function renormalization:

$$\begin{aligned}
\delta Z^{ZZ} &= -\text{Re} \left(\frac{\partial}{\partial k^2} \Sigma_\perp^{ZZ} (k^2) \right)_{k^2=M_Z^2}, & \delta Z^{ZA} &= 2\text{Re} \left(\frac{\Sigma_\perp^{AZ} (0)}{M_Z^2} \right), \\
\delta Z^{AA} &= -\text{Re} \left(\frac{\partial}{\partial k^2} \Sigma_\perp^{AA} (k^2) \right)_{k^2=0}, & \delta Z^{AZ} &= -2\text{Re} \left(\frac{\Sigma_\perp^{AZ} (M_Z^2)}{M_Z^2} \right), \\
\delta Z^{WW} &= -\text{Re} \left(\frac{\partial}{\partial k^2} \Sigma_\perp^{WW} (k^2) \right)_{k^2=M_W^2}, & \delta Z^H &= -\text{Re} \left(\frac{\partial}{\partial k^2} \Sigma^H (k^2) \right)_{k^2=M_H^2},
\end{aligned} \tag{3.3}$$

$$\begin{aligned}
\delta Z^\chi &= -\text{Re} \left(\frac{\partial}{\partial k^2} \Sigma^\chi (k^2) \right)_{k^2=M_Z^2}, & \delta Z^\phi &= -\text{Re} \left(\frac{\partial}{\partial k^2} \Sigma^\phi (k^2) \right)_{k^2=M_W^2}, \\
\delta Z_{ii}^{f,L} &= -\text{Re} \left(\Sigma_{ii}^{f,L} (m_{f_i}^2) \right) \\
&\quad - m_{f_i}^2 \text{Re} \left(\frac{\partial}{\partial p^2} \left[\Sigma_{ii}^{f,L} (p^2) + \Sigma_{ii}^{f,R} (p^2) + 2\Sigma_{ii}^{f,S} (p^2) \right] \right)_{p^2=m_{f_i}^2}, \\
\delta Z_{ii}^{f,R} &= -\text{Re} \left(\Sigma_{ii}^{f,R} (m_{f_i}^2) \right) \\
&\quad - m_{f_i}^2 \text{Re} \left(\frac{\partial}{\partial p^2} \left[\Sigma_{ii}^{f,L} (p^2) + \Sigma_{ii}^{f,R} (p^2) + 2\Sigma_{ii}^{f,S} (p^2) \right] \right)_{p^2=m_{f_i}^2}.
\end{aligned}$$

Mass renormalization:

$$\begin{aligned}
\delta M_Z^2 &= \text{Re} \left(\Sigma_\perp^{ZZ} (M_Z^2) \right), & \delta M_W^2 &= \text{Re} \left(\Sigma_\perp^{WW} (M_W^2) \right), \\
\delta M_H^2 &= \text{Re} \left(\Sigma^H (M_H^2) \right), & \delta m_{f_i} &= \frac{1}{2} m_{f_i} \text{Re} \left(\Sigma_{ii}^{f,L} (m_{f_i}^2) + \Sigma_{ii}^{f,R} (m_{f_i}^2) + 2\Sigma_{ii}^{f,S} (m_{f_i}^2) \right).
\end{aligned} \tag{3.4}$$

Here L and R correspond to left- and right-handed fermions, Σ means one-loop integral of the truncated self-energy graph, and \perp denotes the transverse part only.

Charge and mixing angle renormalization:

$$\begin{aligned}
\delta \sin^2 \theta_W &= \cos^2 \theta_W \left(\frac{\delta M_Z^2}{M_Z^2} - \frac{\delta M_W^2}{M_W^2} \right), & \delta \cos^2 \theta_W &= -\delta \sin^2 \theta_W, \\
\delta e &= -\frac{1}{2} \left(\delta Z^{AA} + \frac{\sin^2 \theta_W}{\cos^2 \theta_W} \delta Z^{ZA} \right),
\end{aligned} \tag{3.5}$$

with $\sin^2 \theta_W = 1 - M_W^2/M_Z^2$.

C. Infrared divergences and soft-photon emission

For diagrams with photon exchange between external fermion legs we have encountered infrared (IR) divergences. These are regulated by introducing a small photon “rest mass” λ in loop integrals involving the photon propagator. This results in $\ln(m_f^2/\lambda^2)$ terms in the amplitude. Hence the radiative corrections are, strictly speaking, infinite in the limit $\lambda \rightarrow 0$. This unphysical dependence on λ is cancelled by adding the inelastic bremsstrahlung contributions arising from soft-photon emission by the external fermions (i.e. from the initial or final electron or quark) to the scattering cross section [20].

To see how this works in the parity-violating asymmetry, consider the inelastic bremsstrahlung amplitude \mathcal{M}_b^Z , which includes the four diagrams of Fig. 3 involving Z exchange, and the corresponding QED amplitude \mathcal{M}_b^γ (not shown) involving photon exchange. The total inelastic cross section is given by

$$d\sigma_b^{eq} \sim \left| \mathcal{M}_b^\gamma + \mathcal{M}_b^Z \right|^2. \tag{3.6}$$

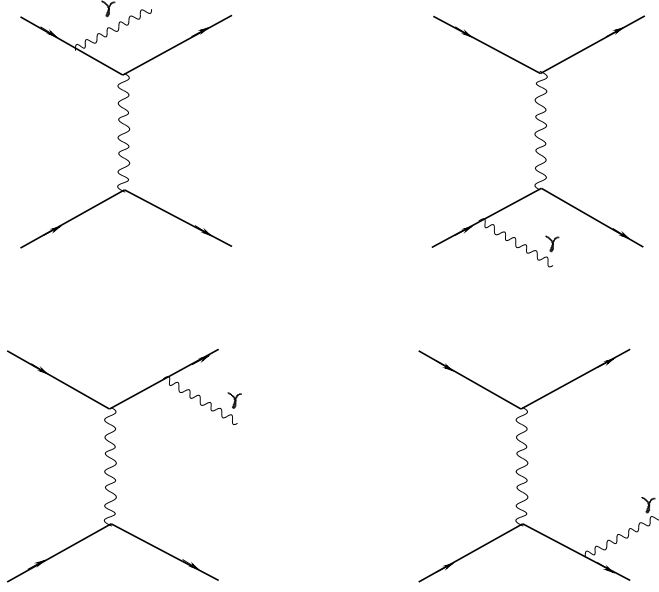


FIG. 3. Bremsstrahlung diagrams for treating IR divergences.

In analogy with Eq. (2.1), a parity-violating asymmetry will result from the interference term $2\text{Re}\{(\mathcal{M}_b^\gamma)^* \mathcal{M}_b^Z\}$.

In the soft photon approximation, it is straightforward to show (see Ref. [21], for example) that the amplitude for soft photon emission can be written in terms of the Born (tree level) amplitude

$$\mathcal{M}_b^\gamma = \mathcal{M}_{\text{Born}}^\gamma \left[-\frac{p_1}{(p_1 \cdot k)} + \frac{p_3}{(p_3 \cdot k)} + \frac{Q_q p_2}{(p_2 \cdot k)} - \frac{Q_q p_4}{(p_4 \cdot k)} \right] \cdot \epsilon^*(k), \quad (3.7)$$

with k the momentum of the photon and $\epsilon(k)$ its polarization. This is just the amplitude for elastic scattering (without bremsstrahlung) times a factor for soft photon emission. An identical factor relates \mathcal{M}_b^Z to $\mathcal{M}_{\text{Born}}^Z$.

The contribution of the parity-violating inelastic differential cross section to the radiative correction can also be expressed in terms of the parity-violating elastic Born cross section, once the appropriate integrals over phase space are done. The steps involved in carrying out the phase space integrals are analogous to ordinary parity-conserving electron scattering, as discussed for example in the paper by Maximon and Tjon [21]. We refer the reader to that paper for details, and simply present the result that

$$d\sigma_b^{eq} = d\sigma_{\text{Born}}^{eq} \kappa_{\text{soft}}^{eq}, \quad (3.8)$$

where $\kappa_{\text{soft}}^{eq}$ is the soft-photon factor defined as

$$\kappa_{\text{soft}}^{eq} = -\frac{\alpha}{2\pi^2} \int_{|\mathbf{k}| \leq \Delta\epsilon} \frac{d^3k}{2\sqrt{\mathbf{k}^2 + \lambda^2}} \left(-\frac{p_1}{(p_1 \cdot k)} + \frac{p_3}{(p_3 \cdot k)} + \frac{Q_q p_2}{(p_2 \cdot k)} - \frac{Q_q p_4}{(p_4 \cdot k)} \right)^2. \quad (3.9)$$

Here $\Delta\varepsilon$ is the maximum momentum of the undetected photon for which an elastic scattering event is recorded. It is related to the final electron detector acceptance in the lab frame, ΔE .

Adding together the elastic and inelastic cross sections, we have

$$d\sigma_{\text{tot}}^{eq} \sim \left| \mathcal{M}_{\text{Born}}^\gamma + \mathcal{M}_{\text{rad}}^\gamma + \mathcal{M}_{\text{Born}}^Z + \mathcal{M}_{\text{rad}}^Z \right|^2 + \left| \mathcal{M}_{\text{Born}}^\gamma + \mathcal{M}_{\text{Born}}^Z \right|^2 \kappa_{\text{soft}}^{eq}, \quad (3.10)$$

where $\mathcal{M}_{\text{rad}}^\gamma$ and $\mathcal{M}_{\text{rad}}^Z$ denote the one-loop radiative corrections. Note that at this stage, our expression (3.10) also includes the purely QED radiative corrections $\mathcal{M}_{\text{rad}}^\gamma$ to the Born amplitude $\mathcal{M}_{\text{Born}}^\gamma$. $\mathcal{M}_{\text{rad}}^\gamma$ includes vertex and $\gamma\gamma$ box diagrams of order $\mathcal{O}(\alpha^2)$.

For the PV contribution, it is convenient to work with the amplitude $\mathcal{M}_{\text{PV}}^{eq}$ defined in Eq. (2.15), from which we can write the relevant PV interference term as

$$d\sigma_{\text{PV,tot}}^{eq} \sim 2\text{Re} \left\{ (\mathcal{M}_{\text{Born}}^\gamma)^* \left(\mathcal{M}_{\text{PV,tree}}^{eq} + \mathcal{M}_{\text{PV,rad}}^{eq} + \mathcal{M}_{\text{PV,tree}}^{eq} \frac{1}{2} \kappa_{\text{soft}}^{eq} \right) + \left(\mathcal{M}_{\text{PV,tree}}^{eq} \right)^* \left(\mathcal{M}_{\text{rad}}^\gamma + \mathcal{M}_{\text{Born}}^\gamma \frac{1}{2} \kappa_{\text{soft}}^{eq} \right) \right\}. \quad (3.11)$$

At this point we note that the second term of Eq. (3.11) involves a PV interference term between $\mathcal{M}_{\text{rad}}^\gamma$ and $\mathcal{M}_{\text{PV,tree}}^{eq}$, plus the soft photon emission contribution needed to cancel the IR divergences in $\mathcal{M}_{\text{rad}}^\gamma$. In principal, one should use the full expression (3.11) to evaluate both the QED and weak radiative corrections on the same footing, since they contribute to the PV asymmetry at the same order. In practice, this has not been done. We take the position here that experimental analyses have already accounted for the QED radiative corrections, and to include such effects again here would be double counting. Accordingly, we drop the second term in Eq. (3.11) from further consideration at this time.

Using the general structure of the PV amplitude in Eq. (2.15), we can rewrite the first term in Eq. (3.11) as

$$d\sigma_{\text{PV,tot}}^{eq} \sim 2\text{Re} \left\{ (\mathcal{M}_{\text{Born}}^\gamma)^* \left[\left(1 + R_A^q + \frac{1}{2} \kappa_{\text{soft}}^{eq} \right) A_{\text{tree}}^{eq} J_{VA}^{eq} + \left(1 + R_V^q + \frac{1}{2} \kappa_{\text{soft}}^{eq} \right) B_{\text{tree}}^{eq} J_{AV}^{eq} \right] \right\}, \quad (3.12)$$

where current products J_{VA}^{eq} and J_{AV}^{eq} are defined in Eq. (2.15).

Evaluating Eq. (3.9), we have

$$\begin{aligned} \kappa_{\text{soft}}^{eq} = & -\frac{\alpha}{2\pi^2} \left[2m_e^2 I(p_1, p_1) - (2m_e^2 - t) I(p_1, p_3) + 2Q_q^2 m_q^2 I(p_2, p_2) \right. \\ & - Q_q^2 (2m_q^2 - t) I(p_2, p_4) - 2Q_q (u - m_e^2 - m_q^2) I(p_1, p_4) \\ & \left. - 2Q_q (s - m_e^2 - m_q^2) I(p_1, p_2) \right], \end{aligned} \quad (3.13)$$

with the soft-photon emission integral $I(p_i, p_j)$ defined as

$$I(p_i, p_j) = \int_{|\mathbf{k}| \leq \Delta\varepsilon} \frac{d^3k}{2\sqrt{\mathbf{k}^2 + \lambda^2}} \frac{1}{(p_i \cdot k)(p_j \cdot k)}. \quad (3.14)$$

These integrals generally have been worked out in Ref. [22]. For electron-quark scattering in the CM frame, we have (see also Ref. [19])

$$\begin{aligned}
I(p_i, p_j) = & \frac{2\pi\alpha_{ij}}{\alpha_{ij}^2 m_i^2 - m_j^2} \left[\frac{1}{2} \ln \left(\frac{\alpha_{ij}^2 m_i^2}{m_j^2} \right) \ln \left(\frac{4\Delta\varepsilon^2}{\lambda^2} \right) + \frac{1}{4} \ln^2 \left(\frac{E_i - p_i}{E_i + p_i} \right) - \frac{1}{4} \ln^2 \left(\frac{E_j - p_j}{E_j + p_j} \right) \right. \\
& + \text{Li}_2 \left(1 - \frac{\alpha_{ij}}{v_{ij}} (E_i + p_i) \right) + \text{Li}_2 \left(1 - \frac{\alpha_{ij}}{v_{ij}} (E_i - p_i) \right) \\
& \left. - \text{Li}_2 \left(1 - \frac{1}{v_{ij}} (E_j + p_j) \right) - \text{Li}_2 \left(1 - \frac{1}{v_{ij}} (E_j - p_j) \right) \right], \tag{3.15}
\end{aligned}$$

where $v_{ij} = (\alpha_{ij}^2 m_i^2 - m_j^2)/(2(\alpha_{ij} E_i - E_j))$, and (E_i, p_i) are the energy and momentum in the CM system. The parameters for different values of i, j are given in Table I. Li_2 is the dilogarithm function

$$\text{Li}_2(z) = \int_z^0 dt \frac{\ln(1-t)}{t}. \tag{3.16}$$

TABLE I. Soft photon emission integral parameters of Eq. (3.15).

i	j	m_i	m_j	α_{ij}
1	1	m_e	m_e	1
2	2	m_q	m_q	1
1	3	m_e	m_e	$1 - \frac{t}{2m_e^2} + \frac{\sqrt{t^2 - 4tm_e^2}}{2m_e^2}$
2	4	m_q	m_q	$1 - \frac{t}{2m_q^2} + \frac{\sqrt{t^2 - 4tm_q^2}}{2m_q^2}$
1	4	m_e	m_q	$\frac{m_e^2 + m_q^2 - u + \sqrt{(u - m_e^2 - m_q^2)^2 - 4m_e^2 m_q^2}}{2m_e^2}$
1	2	m_e	m_q	$\frac{s - m_e^2 - m_q^2 + \sqrt{(m_e^2 + m_q^2 - s)^2 - 4m_e^2 m_q^2}}{2m_e^2}$

The IR divergent ($\ln \lambda$) terms in the elastic and inelastic contributions to the radiative correction cancel exactly. In particular, if we define the modified radiative correction factors

$$\tilde{R}_V^q \equiv R_V^q + \frac{1}{2} \kappa_{\text{soft}}^{eq}, \tag{3.17a}$$

$$\tilde{R}_A^q \equiv R_A^q + \frac{1}{2} \kappa_{\text{soft}}^{eq}. \tag{3.17b}$$

then \tilde{R}_V^q and \tilde{R}_A^q are the radiative corrections to electron-quark scattering free of IR divergences. This was confirmed numerically in our calculation by varying the parameter λ over several orders of magnitude, with no numerically significant change in \tilde{R} .

There remains a weak logarithmic dependence on $\Delta\varepsilon$ of the form $\ln(\Delta\varepsilon/m)$. This dependence will be cancelled if hard photon bremsstrahlung is taken into account. This requires knowledge of particular experimental details such as detector geometry, energy resolution,

phase space cuts, etc. This is beyond the scope of this paper, and we have chosen to simply set the scale for these effects by choosing an energy resolution ΔE corresponding to the parameters of the SAMPLE detector. We leave a more complete treatment of the hard bremsstrahlung corrections, as well as the simultaneous treatment of both QED and weak radiative corrections, as a future project.

IV. NUMERICAL RESULTS

The parameters of the Standard Model are taken from Ref. [23], and are given in Table II. As discussed by Hollik [24], the masses of the light quarks are regarded as parameters, and are adjusted to reproduce the results of a dispersion analysis of the experimentally measured hadronic vacuum polarization.

TABLE II. Standard model parameters used in this calculation.

Quantity	Value	Quantity	Value
m_u	47. MeV	m_e	0.51100 MeV
m_d	47. MeV	m_μ	105.66 MeV
m_s	150. MeV	m_τ	1777.0 MeV
m_c	1.25 GeV	M_Z	91.1882 GeV
m_b	4.2 GeV	M_W	80.419 GeV
m_t	174.3 GeV	M_H	100. GeV

We have chosen the SAMPLE kinematics, corresponding to $E_{e,\text{lab}} = 194$ MeV and an average backward angle $\theta = 146.2^\circ$. Radiative correction results for the $V(e) \times A(q)$ and $A(e) \times V(q)$ current interactions are given separately in the Table III for u , d , and s quarks.

The contributions from self-energy, triangle, and box classes of diagrams are shown for loops which do not involve photons. The self-energy (SE) diagrams give the dominant contribution to radiative corrections in most of the cases. Triangle and box diagrams that involve photon loops are shown as a combined result in column 5 because they are separately infrared divergent. In the combined result, the infrared divergence is cancelled by the bremsstrahlung corrections for soft-photon emission. The corrections show a weak logarithmic dependence on the resolution of the detector, ΔE , which we have taken to be 120 MeV in this table. This corresponds roughly to the parameters of the SAMPLE detector, which detects all electrons above the Čerenkov threshold of 20 MeV [25].

The calculated one-quark radiative corrections were combined to form hadronic vector and axial vector corrections. These are shown in Table IV for the isoscalar and isovector representations $R_V^{T=0}$, $R_V^{T=1}$, $R_A^{T=0}$, and $R_A^{T=1}$. Also shown are the appropriate linear combinations of isoscalar and isovector corrections for the proton (R_V^p and R_A^p) and the neutron (R_V^n and R_A^n). In addition, radiative corrections for the new SAMPLE kinematics, with $E_{\text{lab}} = 120$ MeV and denoted SAMPLE II, are also shown. Differences with the SAMPLE I results are mainly due to the bremsstrahlung corrections.

TABLE III. Radiative corrections for one-quark currents at SAMPLE I kinematics, ($E_{\text{lab}} = 194$ MeV, $\theta = 146.2^\circ$, $\Delta E = 120$ MeV).

$R_{VA}^{ff'}$	Self Energy	Vertex (no γ)	Box (no γ)	Vertex+Box (with γ)	Total
ue	-0.059	-0.015	0.027	0.019	-0.028
de	-0.025	0.026	0.002	0.004	0.008
se	-0.025	0.026	0.002	0.015	0.017
eu	-0.278	-0.224	0.096	0.114	-0.292
ed	-0.278	-0.164	0.022	-0.083	-0.503
es	-0.293	-0.198	0.022	-0.081	-0.550

TABLE IV. Radiative corrections for nucleon currents at SAMPLE I kinematics, ($E_{\text{lab}} = 194$ MeV, $\theta = 146.2^\circ$, $\Delta E = 120$ MeV), and SAMPLE II kinematics ($E_{\text{lab}} = 120$ MeV, $\theta = 146.2^\circ$, $\Delta E = 77$ MeV).

		T=0	T=1	isosinglet	p	n
SAMPLE I	R_V	0.057	-0.005	0.029	-0.252	0.022
	R_A	-0.210	-0.398	-0.760	-0.608	-0.187
SAMPLE II	R_V	0.053	-0.012	0.024	-0.271	0.017
	R_A	-0.216	-0.408	-0.781	-0.624	-0.192

We point out again that these values are calculated in the CDR scheme, and also include a bremsstrahlung contribution. Values calculated in the $\overline{\text{MS}}$ scheme tend to be smaller [7], however the tree level amplitudes also differ between the two schemes due to the different definitions of $\sin^2 \theta_W$.

It is interesting to examine the dependencies of the total radiative corrections $R_A^{T=1}$ and R_V^p on various kinematic and Standard Model parameters. These two corrections are large because the tree level amplitudes are suppressed by $(1 - 4 \sin^2 \theta_W)$. We have found only a weak dependence of the radiative corrections on scattering angle θ and electron energy E_{lab} .

Figure 4 shows the strong dependence of radiative corrections on the mass of the top quark. It also facilitates comparison with previous work [5], which used $m_t = 120$ MeV. This strong dependence on m_t arises from the large mass splitting within the top-bottom fermion doublet. The corrections show only a slight dependence on the Higgs mass M_H , which we have not shown. In Fig. 5 we show the (logarithmic) dependence of R_V^p and $R_A^{T=1}$ on the the photon detection parameter ΔE .

V. EXPERIMENT

The first experiment to measure the weak neutral magnetic form factor G_M^s of the nucleon is the SAMPLE experiment. The details of the techniques employed in this experiment are

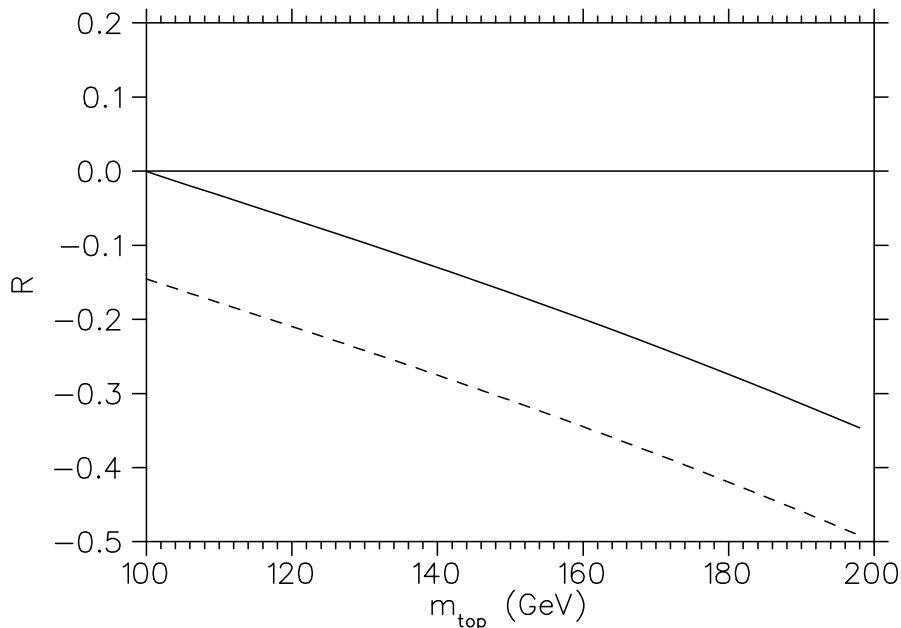


FIG. 4. $R_A^{T=1}$ (dashed line) and R_V^P (solid line) as a function of the mass of the top quark (in GeV).

available in Refs. [10,12,25]. The experiment involves scattering 194 MeV polarized electrons from protons and deuterium. The scattered electrons are detected at 4 backward angles $138^\circ < \theta < 160^\circ$, which results in an average $Q^2 \simeq 0.1(\text{GeV}/c)^2$.

The measured proton and deuteron asymmetries for $Q^2 = 0.1 (\text{GeV}/c)^2$ and $\theta_{\text{avg}} = 146.2^\circ$ are (in ppm):

$$A_p^{\text{exp}} = -4.92 \pm 0.61 \pm 0.73, \quad (5.1a)$$

$$A_d^{\text{exp}} = -6.97 \pm 0.64 \pm 0.55. \quad (5.1b)$$

The first uncertainty is statistical while the second is systematic. In a subsequent analysis, Spayde [26] has reexamined the data, and finds two significant corrections. The first arises from a different treatment of the electromagnetic radiative corrections, while the second is a correction for the fraction of the signal due to pions. Each correction increases A_p and A_d by about 4 percent, resulting in quoted asymmetries of

$$A_p^{\text{exp}} = -5.61 \pm 0.67 \pm 0.88, \quad (5.2a)$$

$$A_d^{\text{exp}} = -7.28 \pm 0.68 \pm 0.75. \quad (5.2b)$$

Our theoretical results for the one quark contributions given in Table IV need to be supplemented by the many quark contributions. These have been evaluated using chiral perturbation theory by Zhu *et al.* [8], who found small, predominantly isovector, contributions. Their isovector contribution can be parameterized as $R_A^{T=1} = -0.06 \pm 0.24$, while the isoscalar is $R_A^{T=0} = -0.01 \pm 0.14$. The quoted uncertainties are large, and dominate the overall uncertainties in the theoretical analysis, as described below.

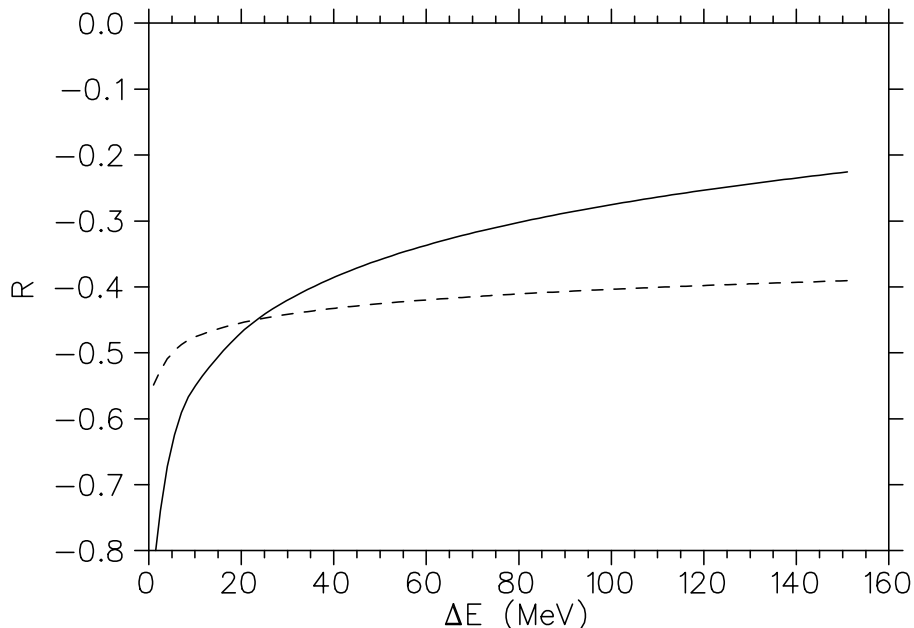


FIG. 5. $R_A^{T=1}$ (dashed line) and R_V^P (solid line) as a function of the photon detection parameter ΔE (in MeV).

Our error analysis for the theoretical asymmetry takes into account uncertainties in the measured electromagnetic form factors, in the axial contributions $G_A^{(8)}$ and G_A^s , and in the radiative corrections. The largest source of uncertainty in the one quark radiative corrections is in the soft photon approximation for the bremsstrahlung contributions. We have allowed for a rather generous error estimate by evaluating these corrections for $\Delta E = 60$ MeV, which is half the value used in Table IV.

Our theoretical asymmetry for the SAMPLE kinematics, including all radiative corrections, and adding errors in quadrature, can be written to show the explicit dependence on the strange form factors:

$$A_p^{\text{th}} = (-7.29 \pm 0.65) + (3.61 \pm 0.07)G_M^s(0.1) + 1.94G_E^s(0.1), \quad (5.3a)$$

$$A_d^{\text{th}} = (-8.74 \pm 0.89) + (0.82 \pm 0.05)G_M^s(0.1) + 1.46G_E^s(0.1). \quad (5.3b)$$

For no strange quark contribution, the measured asymmetries are smaller than the theoretical ones. The discrepancy between the theoretical and experimental values for A_p and A_d are about the same, whereas the coefficients of the dominant G_M^s term are considerably different.

In our analysis we have used the recent nucleon electromagnetic form factors determined by Brash *et al.* [11]. At $Q^2 = 0.1$ GeV, these nucleon form factors tend to be smaller than in the Galster parameterization, thereby exacerbating the discrepancy between theoretical and experimental values noted in previous work [25,26]. The axial form factors are taken to be a simple dipole form, following Refs. [7,25].

The contribution from G_E^s for these kinematics is expected to be small. For the range of values of the strange radius $r_s^2 = \pm 0.22$ found in the literature, we expect $G_E^s(0.1)$ to be in the

range ∓ 0.10 . For comparison, the neutron electric form factor has the value $G_E^n(0.1) = 0.036$. HAPPEX [27] has measured the asymmetry A_p at $\theta = 12.3^\circ$ and $Q^2 = 0.477$. They find the linear combination $(G_E^s + 0.392G_M^s) = 0.025 \pm 0.020 \pm 0.014$, which would seem to favor a positive value of G_E^s . A measurement at $Q^2 = 0.1$ is underway, and could shed some light on the SAMPLE result.

Because the largest overall uncertainty in the theoretical calculations is from $R_A^{T=1}$, it is useful to follow the analysis of the SAMPLE papers [25] and isolate this term explicitly. In this case, we have

$$A_p^{\text{th}} = (-5.93 \pm 0.27) + (3.61 \pm 0.07)G_M^s(0.1) + (2.34 \pm 0.03)G_A^{Z,T=1}(0.1), \quad (5.4a)$$

$$A_d^{\text{th}} = (-7.10 \pm 0.40) + (0.82 \pm 0.05)G_M^s(0.1) + (2.83 \pm 0.04)G_A^{Z,T=1}(0.1). \quad (5.4b)$$

We have dropped the G_E^s terms, and have added (in quadrature) an additional uncertainty ± 0.18 to A_p and ± 0.14 to A_d . The isoscalar terms in G_A^Z , shown in Eq. (2.7) have been absorbed into the constant term. The axial isovector contribution is

$$G_A^{Z,T=1}(0.1) = -(1 + R_A^{T=1})G_A^{T=1}(0.1), \quad (5.5)$$

which has the theoretically expected value $G_A^{Z,T=1}(0.1) = -0.58 \pm 0.27$. This includes the large effect of the one quark axial correction ($R_A^{T=1} = -0.40 \pm 0.02$), and the highly uncertain many quark contribution ($R_A^{T=1} = -0.06 \pm 0.24$) of Ref. [8].

Because the coefficients of $G_A^{Z,T=1}$ in Eqs. (5.4) are roughly equal, changes in $G_A^{Z,T=1}$ will shift A_p and A_d by about the same amount. This is consistent with the uniform discrepancy between theory and experiment in A_p and A_d referred to above, and so it is useful to try to fit the data in this way. However, there may be other explanations for such a uniform discrepancy, including other physics, or systematic errors in the experimental analysis of the kind determined by Spayde [26]. Hence we regard this as simply a device for characterizing the data, and indicating possible directions for explanation.

Solving the pair of equations (5.4) for G_M^s and $G_A^{Z,T=1}$, and using the measured asymmetries from Eq. (5.2), we find

$$G_M^s(Q^2 = 0.1) = 0.16 \pm 0.50, \quad (5.6a)$$

$$G_A^{Z,T=1}(Q^2 = 0.1) = -0.11 \pm 0.49. \quad (5.6b)$$

Combining the errors in the extracted value of G_A^Z and the theoretical value quoted above, the difference is about 1σ .

There is some uncertainty about how to extrapolate $G_M^s(Q^2 = 0.1)$ to $\mu_s = G_M^s(Q^2 = 0)$. A simple dipole form consistent with the proton and neutron magnetic electromagnetic form factors would give $\mu_s = 0.21 \pm 0.65$. Using the extrapolation model proposed by Hemmert *et al.* [28], one instead finds a value of the strange magnetic moment $\mu_s = 0.04 \pm 0.50 \pm 0.07$. Here the last value of the error was introduced in the extrapolation. A negative value of μ_s is consistent with expectations from a number of theoretical models [29–32]. In particular, recent lattice QCD calculations find $\mu_s = -0.16 \pm 0.18$ [31] and $\mu_s = -0.28 \pm 0.10$ [32]. By contrast, a recent SU(3) chiral quark-soliton model gives $\mu_s = 0.074$ to 0.115 [33].

We have repeated the above analysis for the SAMPLE II kinematics ($E = 120$ MeV). This experiment is currently being analyzed. We find

$$A_p^{\text{th}} = (-2.13 \pm 0.08) + (1.07 \pm 0.02)G_M^s(0.043) + (1.06 \pm 0.01)G_A^{Z,T=1}(0.043), \quad (5.7a)$$

$$A_d^{\text{th}} = (-2.62 \pm 0.13) + (0.26 \pm 0.02)G_M^s(0.043) + (1.35 \pm 0.01)G_A^{Z,T=1}(0.043), \quad (5.7b)$$

with the theoretically expected value $G_A^{Z,T=1}(0.043) = -0.62 \pm 0.28$. The overall asymmetries are smaller, and the uncertainties enter somewhat differently than in the SAMPLE I kinematics. This should help in determining the role of $G_A^{Z,T=1}$ in the asymmetries.

VI. SUMMARY

We have reexamined the one-loop radiative corrections to the one-quark amplitudes in the CDR scheme. Our calculations include an evaluation of bremsstrahlung corrections in the soft photon approximation. The bremsstrahlung corrections cancel infrared divergences in the one-loop diagrams. The soft photon approximation has a logarithmic dependence on detection threshold. The sensitivity to this parameter will be reduced if hard bremsstrahlung photons are included, but that requires knowledge of the particular experimental setup.

Although we find that $G_A^{Z,T=1}$ is highly suppressed, there is no indication from the present calculation that it is suppressed by the magnitude indicated by the SAMPLE analysis. A contribution from the isosinglet strange axial form factor G_A^s is unlikely to resolve the problem, as we find it is highly suppressed by the isosinglet radiative corrections $R_A^{(0)} = -0.760$. The many quark corrections calculated by Zhu *et al.* [8] were numerically small, but given the large uncertainties, this is one avenue for further theoretical work. Further experimental measurements by the HAPPEX collaboration at $Q^2 = 0.1 \text{ GeV}^2$, as well as a new measurement by the SAMPLE group at the smaller electron energy 120 MeV, should also shed light on this situation.

ACKNOWLEDGMENTS

This work was supported in part by the Natural Sciences and Engineering Research Council of Canada, and by the US Department of Energy. The Southeastern Universities Research Association (SURA) operates the Thomas Jefferson National Accelerator Facility under DOE contract DE-AC05-84ER40150. PGB would like to acknowledge and thank the theory group at Jefferson Lab for support during a sabbatical leave, where part of this work was completed.

REFERENCES

- [1] D.H. Beck and R.D. McKeown, *Ann. Rev. Nucl. Part. Sci.* **51**, 189 (2001).
- [2] D. Kaplan and A. Manohar, *Nucl. Phys.* **B310**, 527 (1988).
- [3] D.H. Beck, *Phys. Rev. D* **39**, 3248 (1989).
- [4] M.J. Musolf, Ph.D. thesis, Princeton University, (1989).
- [5] M.J. Musolf and B.R. Holstein, *Phys. Lett. B* **242**, 461 (1990).
- [6] M.J. Musolf and B.R. Holstein, *Phys. Rev. D* **43**, 2956 (1991).
- [7] M.J. Musolf, T.W. Donnelly, J. Dubach, S.J. Pollock, S. Kowalski, and E.J. Beise, *Phys. Rep.* **239**, 1 (1994).
- [8] S.-L. Zhu, S.J. Puglia, B.R. Holstein, and M.J. Ramsey-Musolf, *Phys. Rev. D* **62**, 033008 (2000).
- [9] T. Hahn and M. Perez-Victoria, *Comp. Phys. Comm.* **118**, 153 (1999).
- [10] D.H. Beck and B.R. Holstein, hep-ph/0102053 (2001).
- [11] E.J. Brash, A. Kozlov, Sh. Li, and G.M. Huber, *Phys. Rev. C* **65** 051001, (2002).
- [12] E.J. Beise, *et al.*, Proc. SPIN96 Symp., Amsterdam, Sept. 1996, nucl-ex/9610011 (1996).
- [13] B.W. Filippone and X. Ji, *Adv. Nucl. Phys.* **26**, 1 (2001).
- [14] T. Hahn, hep-ph/0005029 (2000).
- [15] F. del Aguila *et al.*, *Nucl. Phys.* **B537**, 561 (1999).
- [16] W. Siegel, *Phys. Lett. B* **84**, 193 (1979).
- [17] R. Harlander and M. Steinhauser, *Prog. Part. Nucl. Phys.* **43**, 167 (1999).
- [18] G. Passarino and M. Veltman, *Nucl. Phys.* **B160**, 151 (1979).
- [19] T. Hahn, Ph.D. thesis, University of Karlsruhe, (1997).
- [20] F. Bloch and A. Nordsieck, *Phys. Rev.* **37** (1937) 54.
- [21] L.C. Maximon and J.A. Tjon, *Phys. Rev. C* **62**, 054320 (2000).
- [22] G. 't Hooft and M. Veltman, *Nucl. Phys.* **B153**, 365 (1979).
- [23] Particle Data Group, D.E. Groom *et al.*, *Eur. Phys. J.* **C15**, 1 (2000).
- [24] W.F. Hollik, *Fortsch. Phys.* **38**, 165 (1990).
- [25] B.A. Mueller *et al.*, *Phys. Rev. Lett.* **78**,3824 (1997);
D.T. Spayde *et al.*, *Phys. Rev. Lett.* **84**,1106 (2000).;
R. Hasty *et al.*, *Science* **290**, 2117 (2000).
- [26] D.T. Spayde, Ph.D. thesis, University of Maryland, (2001).
- [27] K.A. Aniol *et al.*, *Phys. Lett. B* **509**, 211 (2001).
- [28] T.R. Hemmert, U.-G. Meissner, and S. Steinberg, *Phys. Lett. B* **437** 184, (1998).
- [29] R.L. Jaffe, *Phys. Lett. B* **229**, 275 (1989).
- [30] S.J. Dong, K.F. Liu, and A.G. Williams, *Phys. Rev. D* **58**, 074504 (1998).
- [31] D.B. Leinweber and A.W. Thomas, *Phys. Rev. D* **62**, 074505 (2000).
- [32] N. Mathur and S.-J. Dong, *Nucl. Phys. Proc. Suppl.* **94**, 311 (2001).
- [33] A. Silva, H.-C. Kim, and K. Goeke, *Phys. Rev. D* **65**, 014016 (2002).